Principle investigation on advanced absorption power generation cycles

Energy Conversion and Management 150 (2017) 800–813

Contents lists available at ScienceDirect

Energy Conversion and Management

journal homepage: www.elsevier.com/locate/enconman

Principle investigation on advanced absorption power generation cycles

Zhiwei Ma, Huashan Bao *, Anthony Paul Roskilly

Sir Joseph Swan Centre for Energy Research, Newcastle University, Newcastle-upon-Tyne NE1 7RU, UK

ARTICLE INFO

Article history:
Received 9 December 2016
Received in revised form 2 February 2017
Accepted 25 February 2017
Available online 7 March 2017

Keywords:
Absorption power generation
Double-effect cycle
Half-effect cycle
Ejector-combined cycle
Efficiencies
Power output

ABSTRACT

Aiming at exploring advanced absorption power generation (APG) cycles using ammonia-water as working solution, the present study has studied one double-effect, one half-effect and one ejector-combined APG cycles based on one of the most widely studied APG cycles – Kalina KCS-11. The performance of these advanced cycles were numerically analyzed and compared against KCS-11 in terms of power output, energy and exergy efficiencies. An optimal mass fraction of ammonia-water solution used in KCS-11 has been identified to achieve the maximum energy and exergy efficiencies, which were 0.09–0.14 and 0.65–0.72 respectively when using 70.0–100.0 °C boiling temperature; however, the corresponding power output was only 23.0–48.0% of its maximum potential. The double-effect APG cycle could effectively improve the energy and exergy efficiencies by 3.6–12.6%, 10.7–28.2% and 19.0–900.0% respectively when using 100.0 °C, 120.0 °C and 140.0 °C boiling temperature; but its power output capacity was about 43.0–63.0% lower. The half-effect cycle could provide larger pressure ratio for power generation, which amplified the power output by 50.0–85.0% but sacrificed its energy and exergy efficiencies by 4.0–45.0% compared to that of KCS-11. To pursue higher energy and exergy efficiencies without a bulky two-stage system, one can replace the throttling valve and mixer in KCS-11 by an ejector to form a ejector-combined APG cycle, which could improve the system energy efficiency by 2.9–6.8% when using 80.0–100.0 °C boiling temperature, while the power output capacity was only slightly influenced.

1. Introduction

The global fossil energy usage grows rapidly in the last few decades, resulting in severe economic and environmental issues. A great deal of research efforts have been made on using the enormous amount of renewable thermal energy sources, such as solar energy and geothermal energy, as well as industrial waste heat, directly or converting them to electricity through diverse technologies [1,2]. As one of effective and environmental-friendly technologies to recover low-grade heat, absorption power generation (APG) cycle has been investigated widely for decades [3,4]. The usage of binary working fluid leads to lower heat transfer temperature difference between the heat source and the working fluid, thereby reducing the thermodynamic irreversibility.

In a pioneering work on APG cycle using ammonia-water as working solution reported by Maloney and Robertson (M-R cycle) [5], a typical absorption refrigeration configuration was modified by removing the condenser and evaporator but connecting a turbine in between the generator and absorber. It was concluded that there was no significant thermodynamic advantage of such APG system over steam Rankine system. That was attributed to the much higher energy loss in the ammonia-water absorption process than that in pure water condensation process in steam Rankine system. Kalina [6] proposed an alternative APG cycle which added one condenser and one pump compared to the M-R cycle. Numerically analysis has revealed that the Kalina cycle can potentially generate 1.4 times power comparing to steam Rankine cycle using the same heat source [7]; compared to M-R cycle, the additional condenser introduces one extra degree of freedom to Kalina cycle, leading to lower energy loss in absorber and then higher cycle efficiency [8]. Based on the original Kalina cycle, various configurations have been proposed to form the Kalina cycle family, including KCS-11, KCS-12, KCS1-2, KCS-34, KCS-34g, and Kalina split-cycle system, where KCS-11 and KCS-34 are the two most widely investigated cycles [3].

KCS-11 has very similar configuration as M-R cycle, but replaces the absorber by one mixer and one condenser. Hettiarachchi et al. [9] concluded that KCS-11 generally had better heat source and working fluid utilization efficiencies comparing to organic Rankine cycle (ORC), and also there existed an optimal ammonia mass fraction of the basic working solution to yield best system energy efficiency at a given turbine inlet pressure. Sun et al. [10–12] numerically studied a solar-driven KCS-11 system with an auxil-

* Corresponding author.
E-mail address: huashan.bao@newcastle.ac.uk (H. Bao).

http://dx.doi.org/10.1016/j.enconman.2017.02.078
0196-8904/

Nomenclature

h	enthalpy (J/kg)
$\dot{m}$	mass flow rate (kg/s)
P	pressure (Pa)
$\dot{Q}$	heating rate (W)
T	temperature (°C)
ΔT_{LMTD}	logarithmic mean temperature difference (°C)
UA	heat exchanger performance (W/K)
V	flow velocity (m/s)
w	mass fraction (–)
$\dot{W}$	power output (W)
η	efficiency (–)

Subscripts

bas	basic
boi	boiler
d	diffuser
en	energy
ex	exergy
H	high pressure/temperature
l	liquid
L	low pressure/temperature
M	medium pressure/temperature
n	nozzle
pump	pump
re	recuperator
rec	rectifier
s	isentropic/suction
tur	turbine
v	vapour

iary super-heater placed at the upstream of the turbine, which could achieve an energy efficiency of 8.93%, about 21.8% higher than that of Rankine system under the same boundary conditions [11]. Singh and Kaushik [13] reported the utilization of KCS-11 in coal-fire steam power plant for waste heat recovery. KCS-11 cycle could have the maximum thermal efficiency at 12.95% when its turbine inlet pressure was at 40.0 bar and the basic working solution had the ammonia mass fraction at 0.8, ultimately the overall energy efficiency of the coal-fire power plant was improved by 0.277%. Elsayed et al. [14] revealed that the KCS-11 using the ammonia-water solution with 0.55 ammonia mass fraction could achieve 20.0–40.0% higher thermal efficiency than that of ORC under the conditions of 15.0 bar turbine inlet pressure, 100.0 °C heat source and 10.0 °C heat sink. He et al. [15] modified KCS-11 by substituting the throttle valve that located between the separator and the mixer for a two-phase expander to pursue more power output, as a result, 2.07–9.39% improvement in thermal efficiency was achieved when the turbine inlet pressure was in the range of 15.0–30.0 bar and the heat source temperature was at 127.0 °C.

Contrasted with KCS-11, KCS-34 has one more recuperator as low pressure recuperator located between the condenser and mixer [16–19], while in some studies it also has one more liquid-vapour separator before the condenser [16,18] which aims to achieve better heat and mass transfer in the condenser. KCS-34 has been applied in practice in a geothermal power plant in Húsavík, Iceland since 2000 [16], and the system using ammonia-water solution with ammonia mass fraction at 0.82 had an energy efficiency of 20.0–25.0% higher than that of ORC system. Many numerical or simulation studies about KCS-34 have been conducted, some have concluded the prominent superiority of KCS-34 to ORC with some case studies [16,17], while some argued about marginal efficiency improvement by KCS-34 and also expressed the concerns about the more complicated and costly configuration of KCS-34 [18,19].

On the other side, there are plenty of advanced absorption cycles [20,21], such as double-effect, half-effect, sorption-resorption, absorber-heat-recovery, ejector-combined absorption, and diffusion absorption, which are expected to work at higher efficiency or at larger temperature lifting or at other improved aspects. It is worthy of exploring the feasibility and application of such advanced absorption cycles to the APG cycle; however, except one publication on ejector-combined APG cycle [22], such investigation has not been reported yet according to the authors' best knowledge. The present work has studied three different advanced APG cycles based on KCS-11, including one double-effect cycle, one half-effect cycle and one ejector-combined cycle, the corresponding performance including work output, energy efficiency and exergy efficiency were numerically investigated and compared.

2. Working principles of APG cycles and analysis methods

The system schematic and enthalpy-mass fraction (h-w) diagrams of different APG cycles studied in this work are depicted with exemplified operational conditions. The condensation lines and boiling lines of ammonia-water solution were calculated using the equations given by El-Sayed and Tribus [23], while the enthalpies and entropies were calculated based on the Gibbs free energy formulations reported by Ziegler and Trepp [24].

The performance of different APG cycles has been numerically evaluated and compared based on the following assumptions.

- APG cycles were all operated at steady-state.
- The liquid solution at the outlet of condenser was at saturated state.
- Both the vapour and liquid from the separator were at saturated state.
- Throttling process did not change the enthalpy.
- The mixing process in the mixer was an adiabatic process.
- Pressure drop and heat loss in the system were both neglected.

2.1. KCS-11

The absorber in conventional absorption system is replaced by a mixer and a condenser to form the KCS-11 system as shown in Fig. 1. The mixer is to collect and mix the turbine exhaust and the ammonia-lean liquid from the separator, while the condenser locates at the downstream of the mixer. The ammonia-water solution passing through the condenser, pump, recuperator and the boiler is defined as the basic working solution. The condensed basic solution (10–1) is pumped from the condenser to high pressure by a solution pump (1–2) and pre-heated (2–3) by the ammonia-lean fluid from the separator in a recuperator before it enters a boiler. The boiler generates liquid-vapour two phase ammonia-water mixture (3–4) which is then split to saturated ammonia-rich vapour and saturated ammonia-lean liquid by the separator (4–6, 4–5). The vapour expands through the turbine (6–7) with mechanical energy output while the liquid releases its residual heat in the recuperator (5–8) before being throttled (8–9) and mixing with the turbine exhaust in the mixer (7, 9–10).

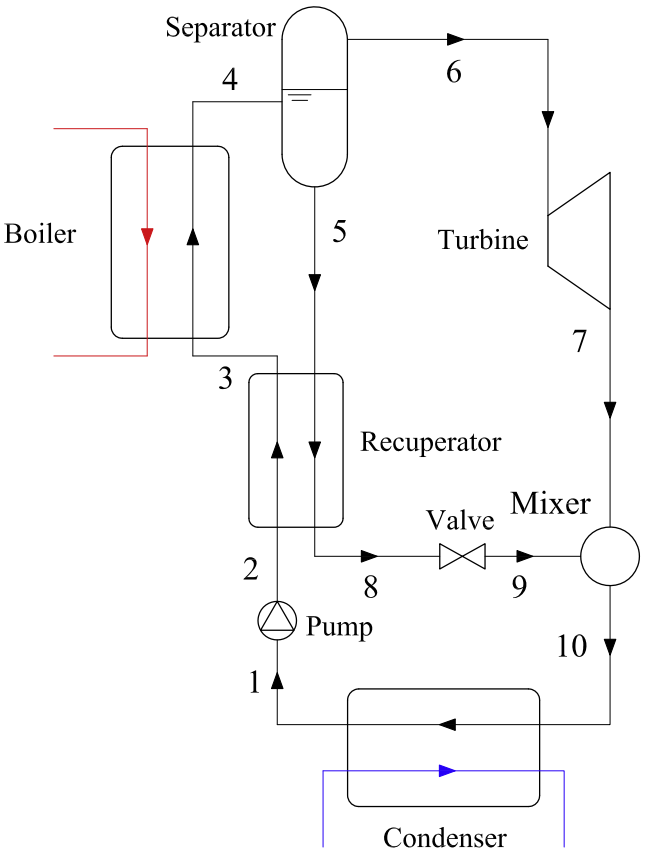

Fig. 1. Schematic diagram of KCS-11.

A working process example of KCS-11 under the operational conditions of 40.0 bar turbine inlet pressure, 100.0 °C boiling temperature, 25.0 °C condensation temperature, 0.8 ammonia mass fraction of basic solution at 0.01 kg/s flow rate, is shown in Fig. 2. The high working pressure in the cycle, P_H, is the pre-defined turbine inlet pressure; the low working pressure, P_L, can be determined by the boiling line of the basic solution (w_{bas} = 0.8) at condensation temperature (point 1), which is 7.949 bar in this example. The enthalpy h_1 and entropy s_1 of the saturated basic solution at point 1 can be obtained according to its temperature, pressure and mass fraction. The basic working solution is pumped from P_L to P_H, the isentropic efficiency η_{pump} of the solution pump is

$$\eta_{pump} = \frac{h_{2s} - h_1}{h_2 - h_1} \tag{1}$$

where h_{2s} is the solution enthalpy at the pump outlet if the pumping process is isentropic, which can be determined by the state equation considering the basic solution at pressure P_H with an entropy value of s_1. The η_{pump} value is pre-defined at 0.85 in the present study, then h_2 can be calculated by Eq. (1). The consumed pumping power is then calculated by the following equation.

$$\dot{W}_{pump} = \dot{m}_1(h_2 - h_1) \tag{2}$$

The heat-exchange process in the recuperator is governed by the following equations.

$$\dot{Q}_{re} = \Delta T_{LMTD} \cdot UA_{re} \tag{3}$$

$$\Delta T_{LMTD} = \frac{T_5 - T_3 - (T_8 - T_2)}{\ln\left(\frac{T_5 - T_3}{T_8 - T_2}\right)} \tag{4}$$

$$\dot{Q}_{re} = \dot{m}_2(h_3 - h_2) = \dot{m}_5(h_5 - h_8) \tag{5}$$

where $\dot{Q}_{re}$ is the heat transfer rate, ΔT_{LMTD} is logarithmic temperature difference, UA_{re} is the multiplicative product of heat transfer coefficient and heat transfer area of the recuperator. Different values of UA_{re} from tens to thousands have been tried in KCS-11 under the mass flow rate of 0.01 kg/s, and 1000 W/K was used in the end for this study since it was large enough to allow an almost perfect heat recovery in recuperator, further increase of UA_{re} only made negligible change on the overall system performance (e.g. the thermal efficiency change is less than 0.5% as UA_{re} is increased from 1000 W/K to 1500 W/K).

Point 4 is at the boiling temperature ($T_4 = T_{boi}$ = 100 °C in the example), while the pressure is at P_H (40.0 bar) and the solution mass fraction equals to the basic solution mass fraction ($w_4 = w_{bas}$ = 0.8). Thus the enthalpy h_4 can be determined by T_4, P_H and w_{bas}. The consumed boiling heat is calculated by Eq. (6).

$$\dot{Q}_{boi} = \dot{m}_3(h_4 - h_3) \tag{6}$$

In the separator, based on the mixture pressure P_H and temperature T_{boi}, the corresponding ammonia mass fraction of the saturated vapour (point 6) and saturated liquid (point 5) can be derived as 0.9889 and 0.6715 respectively by the state equation, and these two points are the intersection points of the isothermal line of T_{boi} with the boiling line and with the condensation line at pressure P_H, respectively. The mass flow rates of the liquid ($\dot{m}_5$) and vapour ($\dot{m}_6$) can be calculated through the mass balance equations in the separator as given by Eqs. (7) and (8).

$$\dot{m}_4 = \dot{m}_5 + \dot{m}_6 \tag{7}$$

$$\dot{m}_4 w_4 = \dot{m}_5 w_5 + \dot{m}_6 w_6 \tag{8}$$

The power output of the turbine by the vapour expansion process (6–7) is calculated by Eq. (9), while the isentropic efficiency of the turbine is in Eq. (10).

$$\dot{W}_{tur} = \dot{m}_6(h_6 - h_7) \tag{9}$$

$$\eta_{tur} = \frac{h_6 - h_7}{h_6 - h_{7s}} \tag{10}$$

where h_{7s} is the enthalpy at turbine outlet if the expansion process is isentropic and it can be determined by considering point 7 at pressure P_L with an entropy value equal to that of point 6 (s_6). As

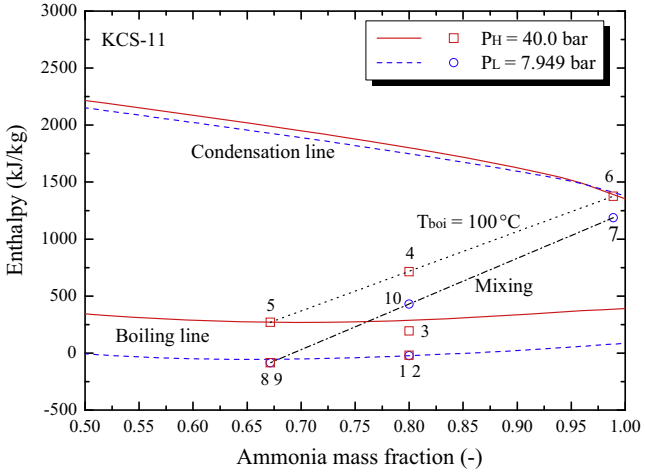

Fig. 2. Operation process of KCS-11 in *h*-*w* diagram, T_{boi} = 100 °C, P_{tur} = 40.0 bar, w_{bas} = 0.8, $\dot{m}_{bas}$ = 0.01 kg/s.

η_{tur} is pre-defined at 0.90 in the present study, the value of h_7 can be obtained by Eq. (10) and it is lower than h_6 as shown in Fig. 2. Thereafter the power output from the turbine can be calculated by Eq. (9). Moreover, it should be mentioned that the vapour quality of the turbine exhaust is assumed to be larger than 0.9 for healthy turbine operation.

The throttling process does not change the fluid enthalpy as expressed in Eq. (11).

$$h_8 = h_9 \tag{11}$$

The mass balance and energy balance equations in the mixer are described by Eqs. (12)–(14) and are used to determine the solution state at point 10.

$$\dot{m}_{10} = \dot{m}_7 + \dot{m}_9 \tag{12}$$

$$\dot{m}_{10} w_{10} = \dot{m}_7 w_7 + \dot{m}_9 w_9 \tag{13}$$

$$\dot{m}_{10} h_{10} = \dot{m}_7 h_7 + \dot{m}_9 h_9 \tag{14}$$

Finally, the energy and exergy efficiencies of the cycle can be evaluated by the following equations.

$$\eta_{en} = \frac{\dot{W}_{tur} - \dot{W}_{pump}}{\dot{Q}_{boi}} \tag{15}$$

$$\eta_{ex} = \frac{\dot{W}_{tur} - \dot{W}_{pump}}{\dot{Q}_{boi}\left(1 - \frac{T_{amb}}{T_{boi}}\right)} \tag{16}$$

2.2. Double-effect APG cycle

There are two types of double-effect absorption heat pump cycle [20], one is parallel type that recovers condensation heat in the high-pressure cycle for the generator in the low-pressure cycle; the other one is called intermediate pressure type which recovers the absorption heat in the high-temperature cycle to heat up the generator in the low-temperature cycle. Since there is no refrigerant condensation/evaporation in APG cycle, only the intermediate pressure type is considered to develop a double-effect APG based on KCS-11 as shown in Fig. 3.

Two sets of KCS-11 are integrated by coupling the condenser (H-Condenser) of one cycle and the boiler (L-Boiler) of the other cycle. These two cycles are referred as low temperature cycle (Low-T cycle) and high temperature cycle (High-T cycle) respectively, yet these two cycles run at the same working pressure but different boiling temperature and using different ammonia mass fraction solutions. In order to ensure effective boiling of the ammonia-water solution in L-Boiler, a relatively ammonia-leaner solution is required in the High-T cycle to guarantee high enough condensation temperature in the High-T cycle if the condensation pressure is fixed.

This double-effect APG system can also use Eqs. (1) to (16) to solve each state point of the High-T and Low-T cycle; it additionally requires the thermal balance in the coupling component, i.e. the L-Boiler/H-Condenser, as expressed in Eq. (17).

$$\dot{m}_{20}(h_{20} - h_{11}) = \dot{m}_3(h_4 - h_3) \tag{17}$$

In current study, high efficient heat exchange is assumed in the L-Boiler/H-Condenser and the temperature difference between the inlet of the condensing solution (T_{20}) and the outlet of the boiling solution (T_4) is pre-defined at 0.5 °C. The ammonia-water solution used in the High-T cycle is considered as the basic working solution for the whole double-effect cycle. The mass flow rate of the basic working solution is pre-defined at 0.01 kg/s, while the solution mass flow rate at the Low-T cycle should be determined iteratively to achieve the thermal balance in Eq. (17).

Fig. 4 exemplifies a double-effect APG cycle under the operational conditions of 20.0 bar turbine inlet pressure, 120.0 °C boiling temperature, 25.0 °C condensation temperature, 0.80 ammonia mass fraction in the Low-T cycle, 0.40 ammonia mass fraction and 0.01 kg/s solution mass flow rate in the High-T cycle. As shown in the figure, the condensation in the High-T cycle results in a 78.7 °C boiling in the Low-T cycle. It is noticed that the specific enthalpy change of the condensation (20–11) in the High-T cycle is less than that of the boiling process (3–4) in the Low-T cycle, which indicates a lower solution mass flow rate in the Low-T cycle (0.0022 kg/s) compared to that of the basic solution in the High-T cycle (0.01 kg/s).

2.3. Half-effect APG cycle

With a pre-defined turbine inlet pressure and fixed condensation temperature, increasing the pressure ratio to pursue productive power generation relies on reducing the condensation pressure, which can be achieved by reducing the ammonia mass fraction of the condensing solution. In this instance, KCS-11 requires higher boiling temperature to generate vapour out from this ammonia-leaner solution to achieve the pre-defined turbine inlet pressure. With two-stage operation, the half-effect cycle has the ability to effectively utilize the ammonia-leaner basic working solution for more power generation without using a higher boiling temperature.

The half-effect APG cycle comprises two sets of KCS-11 integrated by directing the saturated vapour from the separator of the low-pressure cycle (Low-P cycle) to the mixer of the high-pressure cycle (High-P cycle) where it is mixed with the liquid exiting the separator of the High-P cycle, as shown in the schematic diagram of Fig. 5. Such a configuration provides larger pressure ratio for turbine operation with the given heat source temperature. Three pressure levels exist in this half-effect APG cycle, the low pressure P_L at the L-Condenser, the medium pressure P_M at both H-Condenser and L-Boiler, and the high pressure P_H at H-Boiler. Unlike the double-effect APG cycle, both boilers in half-effect APG cycle require heat input and the whole cycle only gains one portion of power output. It is assumed in current study that two boilers operate with the same heat source; since the two condensers are operated at the same condensation temperature, the Low-P cycle solution should have comparatively lower ammonia mass fraction than that of the High-P cycle solution to ensure that P_M in H-Condenser is larger than P_L in L-Condenser. Similar to double-effect APG cycle, the High-P cycle solution was treated as the basic working solution of the whole cycle at the mass flow rate of 0.01 kg/s, while the mass flow rates of the Low-P cycle solution should be determined based on the mass balance as explained below.

To maintain the mass balance between Low-P and High-P cycles and the stable operation of the whole system, the solution at point 6 and 15 must have the same mass flow rate and the same ammonia mass fraction. However, the ammonia-water vapour generated from the L-Boiler is always weaker in ammonia than that generated by H-Boiler because the L-Boiler operates at the same boiling temperature as in H-Boiler ($T_4 = T_{13}$) but at lower boiling pressure ($P_M < P_L$). Therefore a rectifier as illustrated in Fig. 6 must be used instead of a separator to enlarge the mass fraction of ammonia-water vapour from the L-Boiler, leading to the mass balance described as Eqs. (18)–(20).

$$\dot{m}_{4v} = \dot{m}_{6l} + \dot{m}_6 \tag{18}$$

$$\dot{m}_{4v} w_{4v} = \dot{m}_{6l} w_{6l} + \dot{m}_6 w_6 \tag{19}$$

$$\dot{m}_4 w_4 = \dot{m}_{4v} w_{4v} + (\dot{m}_4 - \dot{m}_{4v}) w_{4l} \tag{20}$$

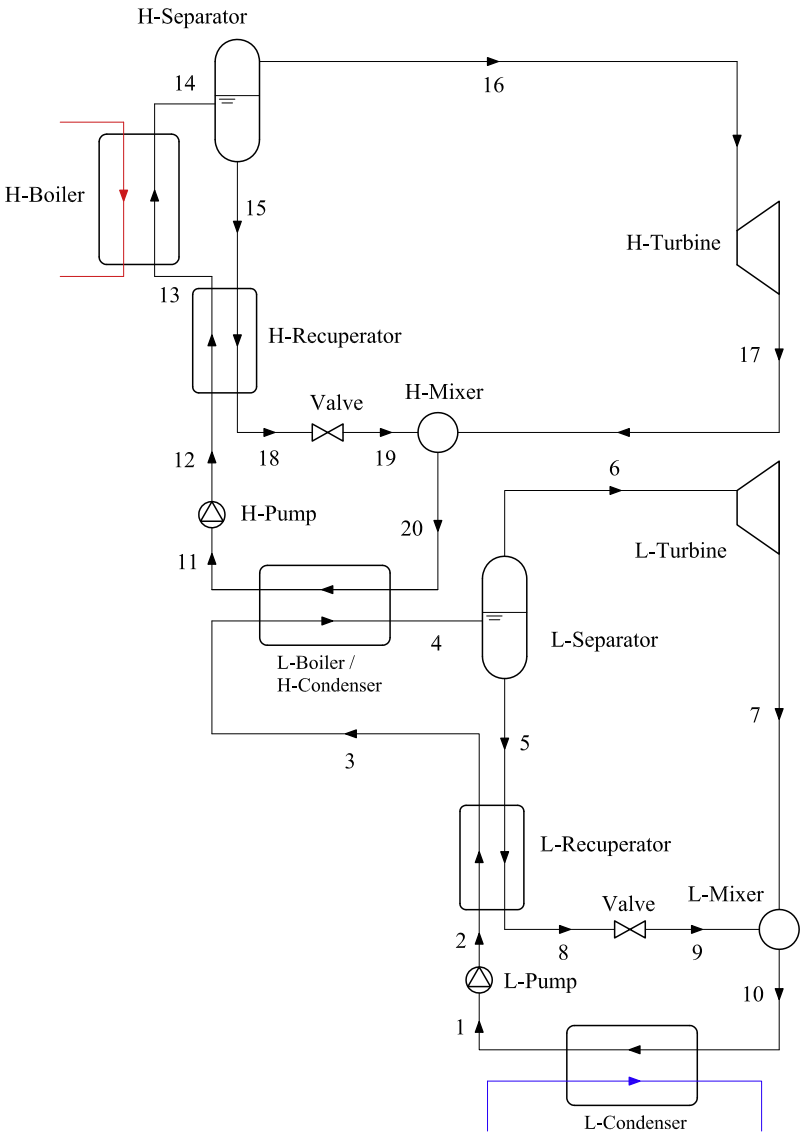

Fig. 3. Schematic diagram of double-effect APG cycle.

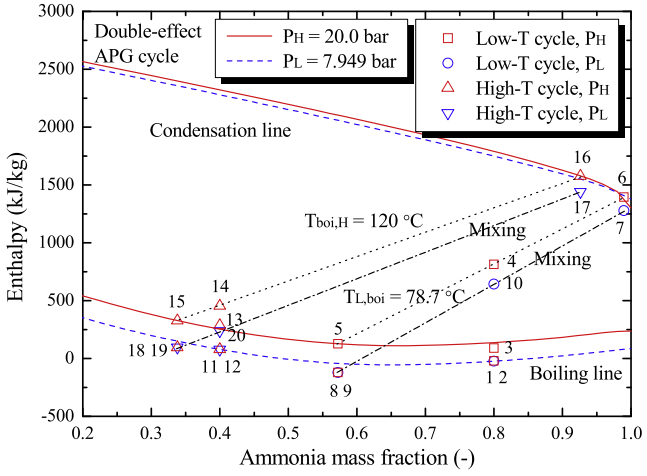

Fig. 4. Operation process of double-effect APG cycle in *h*-*w* diagram, $T_{boi,H}$ = 120.0 °C, P_{tur} = 20.0 bar, $w_{bas,L}$ = 0.8, $w_{bas,H}$ = 0.4, $\dot{m}_{bas,H}$ = 0.01 kg/s.

where the subscripts v and *l* indicate the vapour phase and liquid phase, respectively. The condensation temperature of the rectification can be determined by the mass fraction at point 6, w_6, and the pressure P_M, consequently, the mass fraction of the condensed return liquid, w_{6l}, can be calculated based on this condensation temperature and pressure. Meanwhile, the mass fraction of the saturated vapour and liquid at point 4, w_{4v} and w_{4l} can be calculated on the basis of the boiling temperature, medium pressure P_M and the ammonia mass fraction of the Low-P cycle solution. Thereafter, three unknown parameters, $\dot{m}_4$, $\dot{m}_{4v}$ and $\dot{m}_{6l}$ ($\dot{m}_6$ equals to $\dot{m}_{15}$) are solved through the Eqs. (18)–(20). Further, the energy balance within the rectifier is expressed as Eq. (21), where $\dot{Q}_{rec}$ is the condensation heat released by rectification.

$$\dot{m}_{4v}h_{4v} = \dot{m}_{6l}h_{6l} + \dot{m}_6 h_6 + \dot{Q}_{rec} \tag{21}$$

Fig. 7 depicts a half-effect APG cycle under the conditions of 20.0 bar turbine inlet pressure, 100.0 °C boiling temperature, 25.0 °C condensation temperature, 0.3 ammonia mass fraction in the Low-P cycle solution, 0.6 ammonia mass fraction and 0.01 kg/s solution mass flow rate in the High-P cycle. Three pressure levels at 20.0 bar, 5.1342 bar and 0.9824 bar are built in

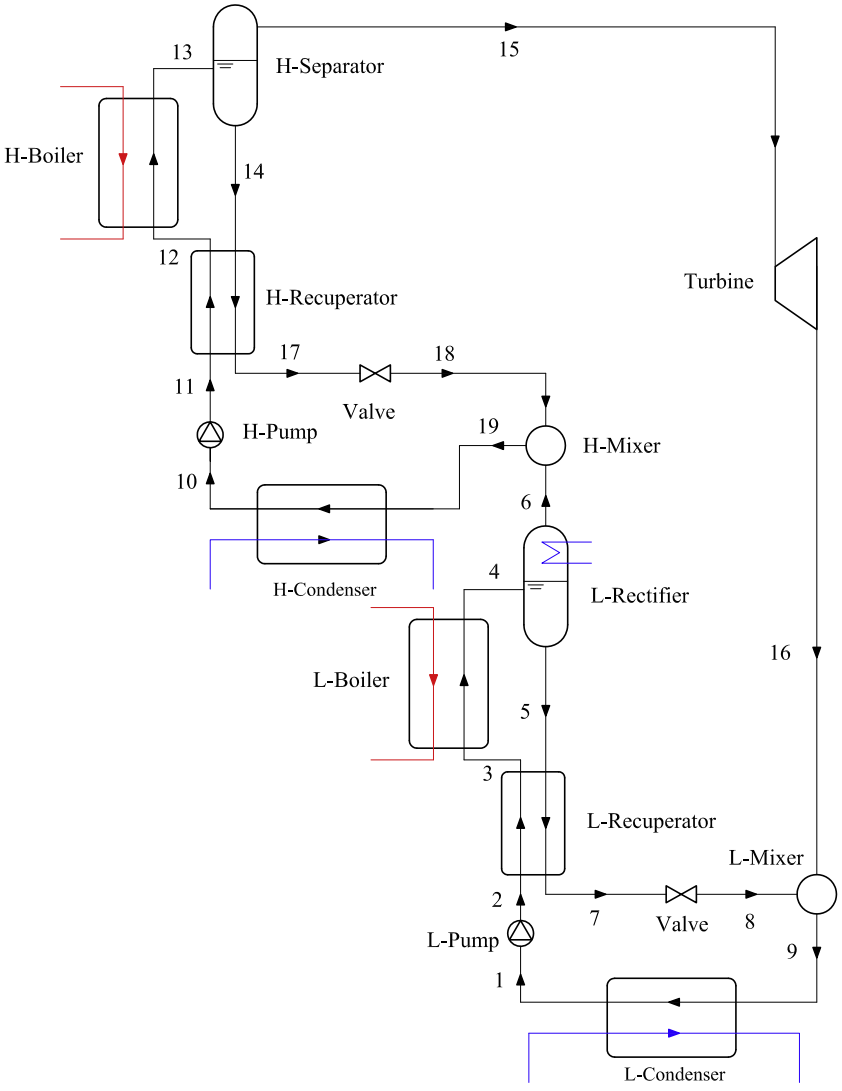

Fig. 5. Schematic diagram of half-effect APG cycle.

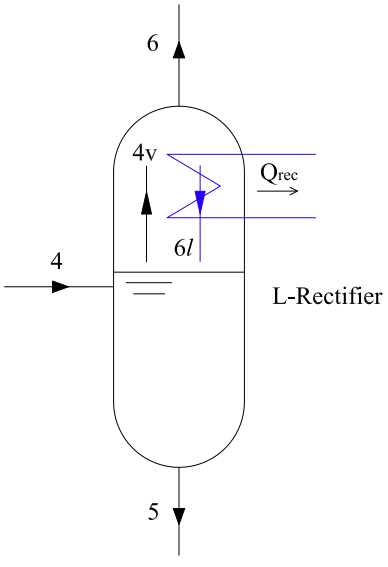

Fig. 6. Schematic diagram of the rectifier used in half-effect APG cycle.

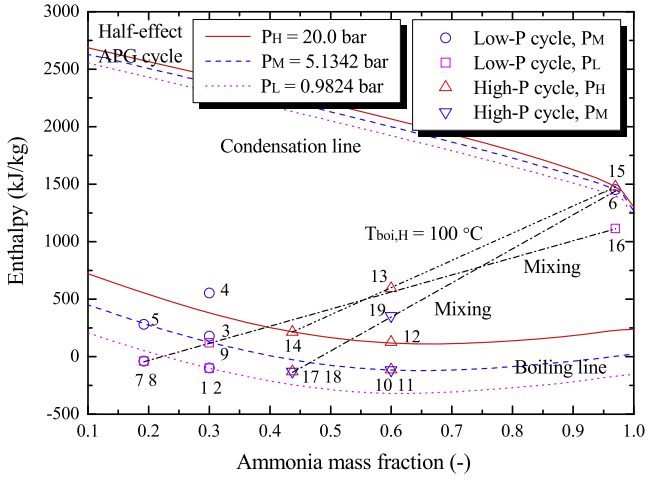

Fig. 7. Operation process of half-effect APG cycle in *h-w* diagram, T_{boi} = 100.0 °C, P_{tur} = 20.0 bar, $w_{bas,L}$ = 0.3, $w_{bas,H}$ = 0.6, $\dot{m}_{bas,H}$ = 0.01 kg/s.

the cycle, indicating a much larger pressure ratio for the turbine than the double-effect APG cycle and KCS-11. Moreover, the connection line of points 4–6 in Fig. 7 is not linear any more due to the usage of L-Rectifier rather than a separator.

2.4. Ejector-combined APG cycle

Based on KCS-11, the ejector-combined APG cycle replaces the throttle valve and the mixer with an ejector as shown in Fig. 8. The employed ejector should be a two-phase ejector since the primary flow from the recuperator is at liquid phase while the turbine exhaust as the secondary flow is at liquid-vapour two phase. By using the ejector, the backpressure of the turbine (point 7 in Fig. 8), P_L, can be lower than the condensation pressure, therefore the power output from the turbine is potentially amplified due to the larger pressure ratio compared to KCS-11.

The analysis of the ejector as schematised in Fig. 9 was based on the following assumptions [25,26].

- The properties and velocities were constant over the cross section of the ejector therefore the analysis was one-dimensional.
- The working fluid was in thermodynamic quasi-equilibrium all the time;
- Viscous pressure drop inside the ejector was negligible.
- The flow velocities outside the ejector in the cycle were negligible compared to the velocities within the ejector.
- Constant pressure in the mixing section was assumed, which should be lower than the pressure of the secondary flow.
- The deviation of the ejection process from the isentropic process could be expressed in terms of non-isentropic efficiencies.

In the suction section, the energy balance equations for the primary and secondary fluid flows are

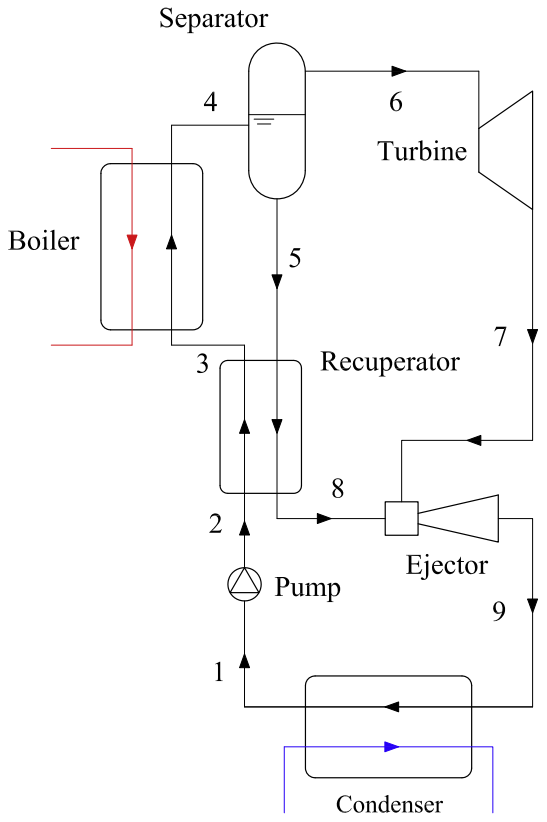

Fig. 8. Schematic diagram of ejector-combined APG cycle.

$$h_8 = h_b + \frac{V_b^2}{2} \tag{22}$$

$$h_7 = h_a + \frac{V_a^2}{2} \tag{23}$$

The efficiency of the nozzle, η_n, and the efficiency of the suction of the secondary fluid, η_s, are given as Eqs. (24) and (25), which are set as 0.75 and 0.9, respectively according to the literature [26,27].

$$\eta_n = \frac{h_b - h_8}{h_{bs} - h_8} \tag{24}$$

$$\eta_s = \frac{h_a - h_7}{h_{as} - h_7} \tag{25}$$

where h_{as} and h_{bs} are the enthalpies at points a and b, respectively in isentropic processes, and they can be calculated based on the pre-defined pressure at mixing section, P_c ($P_a = P_b = P_c$), and the entropies at points 7 and 8.

In the mixing section, the velocity and enthalpy at point c, V_c and h_c, can be determined through the momentum and energy balance equations as Eqs. (26) and (27).

$$(\dot{m}_7 + \dot{m}_8)V_c = \dot{m}_7 V_a + \dot{m}_8 V_b \tag{26}$$

$$(\dot{m}_7 + \dot{m}_8)\left(h_c + \frac{V_c^2}{2}\right) = \dot{m}_7 h_7 + \dot{m}_8 h_8 \tag{27}$$

The energy balance equation of the diffusion process is given as Eq. (28).

$$h_9 = h_c + \frac{V_c^2}{2} \tag{28}$$

Once the enthalpy value at point 9 is identified, the isentropic enthalpy at point 9, h_{9s}, can be calculated by the Eq. (29) based on the pre-defined diffusion efficiency, η_d, at 0.9 [26–27].

$$\eta_d = \frac{h_{9s} - h_c}{h_9 - h_c} \tag{29}$$

Finally the pressure at point 9, i.e. the P_M in this APG cycle, can be determined by h_{9s} and the entropy at point c.

The calculation of ejector-combined APG cycle was initiated based on a hypothetic value of P_L ($P_7 = P_L$) and iterated until the obtained ejector outlet pressure was equal to the condensation pressure. An operation example of the combined-ejection APG cycle is shown in Fig. 10, where it has the turbine inlet pressure at 40.0 bar, boiling temperature at 100.0 °C, condensation temperature at 25.0 °C, and the basic solution at 0.74 ammonia mass fraction and 0.01 kg/s mass flow rate. The condensation pressure is at 7.2116 bar, and the usage of ejector allows a lower turbine backpressure at 6.6692 bar, thus there is the potential to improve both the power output and the thermal efficiency.

3. Results and discussion

The parameters used in current calculation of different APG cycles are presented in Table 1. Initially, the ammonia mass fraction of the basic working solution was varied from 0 to 1 for all studied cases, however, the feasible mass fraction was strongly limited by other working conditions, such as turbine inlet pressure and boiling temperature, so that the different ranges of mass fraction values for different cycles are listed in the table.

Since there is very limited experimental or demonstrational APG systems reported so far, the present calculation is validated against other numerical studies [9,28], as shown in Fig. 11. The energy efficiencies of the KCS-11 obtained in the current work

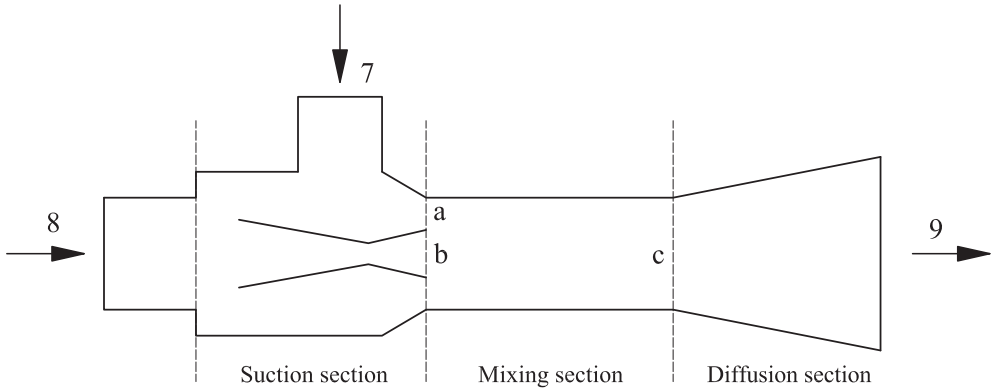

Fig. 9. Schematic diagram of the ejector used in ejector-combined APG cycle.

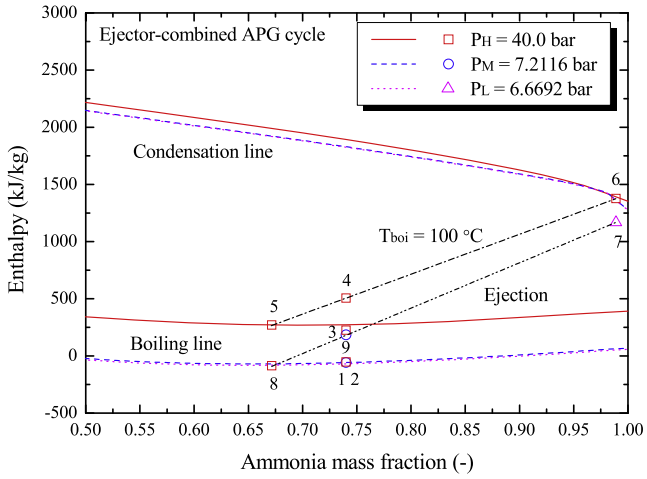

Fig. 10. Operation process of ejector-combined cycle in *h-w* diagram, T_{boi} = 100.0 °C, P_{tur} = 40.0 bar, w_{bas} = 0.74, $\dot{m}_{bas}$ = 0.01 kg/s.

exhibit the same variation tendencies with other reported results under the same conditions: with the given boiling temperature, higher turbine inlet pressure is associated with larger ammonia mass fraction of the basic working fluid; there is always a peak value of energy efficiency at certain ammonia mass fraction on each condition curve. However, the results of the current work are slightly higher than others, especially when the basic ammonia mass fraction is relatively lower. This can be explained by the high UA_{re} value used in the present calculation, which maximizes the heat recovery in the recuperator and therefore improves the energy efficiency. The open symbols in the figure are the energy efficiencies of ORC using ammonia as working fluid calculated by the present study by removing separator, recuperator, valve and mixture from KCS-11. These efficiencies are obviously lower than the maximum efficiencies by using optimal ammonia-water solution in KCS-11; and lower turbine inlet pressure leads to more improvement on energy efficiency by using KCS-11. This comparison validates the superiority of KCS against ORC at the same working condition.

3.1. KCS-11

Fig. 12(a)–(c) shows the power output, energy efficiency and exergy efficiency of KCS-11 varying with different basic ammonia mass fraction, while the turbine inlet pressure is at 10.0 bar, 20.0 bar and 30.0 bar, the boiling temperature is in the range from 70.0 to 100.0 °C. With the provided boiling temperature and turbine inlet pressure, using ammonia-leaner solution leads to lower condensation pressure and therefore larger pressure ratio for power generation; however, less amount of ammonia vapour can be generated from the ammonia-leaner solution, which leads to smaller power generation. The balance of these two conflicting phenomena reflected on the variation of power output is shown in Fig. 12(a). The optimal mass fraction marked by star symbols on each curve is identified based on the maximum energy and exergy efficiency presented in Fig. 12(b) and (c). These optimal efficiency points never accompany with the maximum power output, but only achieve around 23.0–48.0% of maximum power output and locate in the lower-mass-fraction part of each curve.

The usage of ammonia-leaner basic working solution reduces the required boiling heat because less vapour can be generated with given boiling temperature and turbine inlet pressure, and meanwhile more return liquid from the separator allows more heat recovered in the recuparator, therefore the energy efficiency generally increases with the decreasing ammonia mass fraction as shown in Fig. 12(b). However, the energy efficiency starts to decrease once the ammonia mass fraction is lower than a certain

Table 1
Working conditions of different APG cycles studied in present paper.

	KCS-11	Double-effect APG cycle	Half-effect APG cycle	Ejector-combined APG cycle
P_{tur} (bar)	10–60	10–30	10–40	20–40
T_{boi} (°C)	70–140	100–140	60–100	70–100
w_{bas} (–)[a]	0.3–0.98	0.5–0.9 (Low-T) 0.3–0.8 (High-T)	0.2–0.9 (Low-P) 0.35–0.95 (High-P)	0.44–0.94
$\dot{m}_{bas}$ (kg/s)	0.01	0.01 (High-T)	0.01 (High-P)	0.01
T_{con} (°C)	25			
UA_{re} (W/K)	1000			
η_{tur} (–)	0.90			
η_{pump} (–)	0.85			

[a] The varying of ammonia mass fraction was initially set from 0 to 1, however, the feasible mass fraction was limited by working conditions at each cycle.

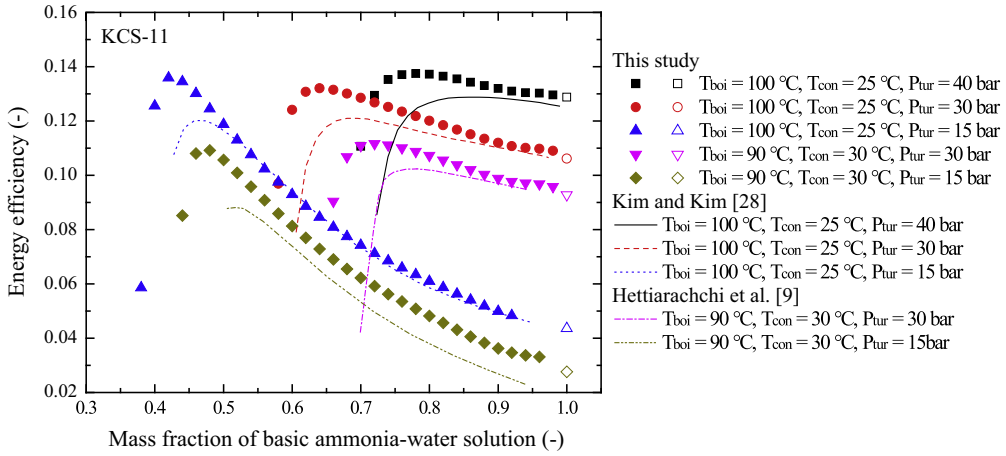

Fig. 11. Validation of present calculation by the comparison with other numerical results based on KCS-11.

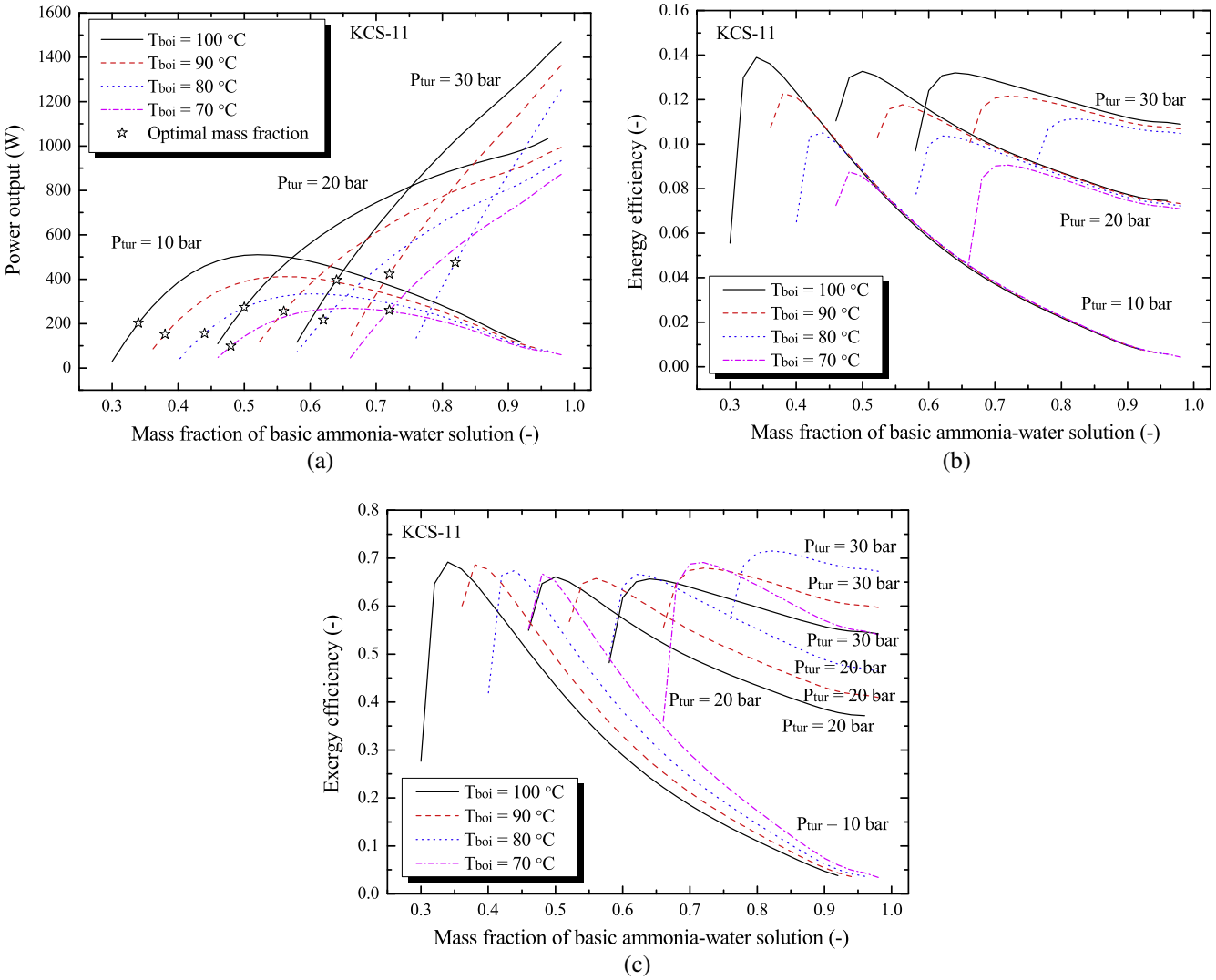

Fig. 12. Performance of KCS-11, (a) power output; (b) energy efficiency; (c) exergy efficiency.

value, which can be attributed to that the generated net power is reducing towards null as less and less vapour is generated, but at the same time the boiler still consumes certain amount of sensible heat, then the efficiency calculated by Eq. (15) should decrease to zero eventually. That indicates there exists an optimal ammonia mass fraction of the basic solution to yield the maximum cyclic energy efficiency with the given boiling temperature and turbine inlet pressure. In the figure, the curves of higher turbine inlet pres-

sure have relatively higher optimal mass fraction compared to those of lower turbine inlet pressure, which is in line with the fact that ammonia-richer solution has higher working pressure. Higher boiling temperature can generate vapour from ammonia-leaner solution, conversely, therefore the feasible range of ammonia mass fraction for higher boiling temperature is wider than that with lower boiling temperature.

When the turbine inlet pressure is lower, the ammonia mass fraction of the used solution has greater impact on the energy efficiency, e.g. the energy efficiency changes from 0.14 to 0.01 over the whole range of mass fraction studied at 10.0 bar turbine inlet pressure, whereas there is only 0.04 difference between the maximal and the minimal efficiencies when turbine inlet pressure is at 30.0 bar. That suggests if the turbine inlet pressure is sufficiently high, prioritising the power output unnecessarily leads to poor energy efficiency but still has the energy efficiency in the reasonably acceptable range. For example, the power output can be improved from about 423.1 W to 1362.7 W while the energy efficiency only drops from 0.122 to 0.107 when pursuing maximum power output rather than maximum efficiency at the condition of 90.0 °C boiling temperature and 30.0 bar turbine inlet pressure. The performance comparison between these two strategies under different conditions is presented in Table 2.

The exergy efficiency in Fig. 2(c) is found to have the similar variation tendency as the energy efficiency, and the corresponding optimal mass fractions are exactly the same with those of energy efficiency identified in Fig. 12(b). The maximum value of exergy efficiency is in the range of 0.65–0.72 with the highest value under the conditions of 80.0 °C boiling temperature, 30.0 bar turbine inlet pressure and 0.82 ammonia mass fraction. Moreover, using lower boiling temperature generally leads to higher exergy efficiency.

3.2. Double-effect APG cycle

As an example with 100.0 °C boiling temperature, Fig. 13(a)–(c) show the power output, energy and exergy efficiencies of the double-effect APG cycle against the ammonia mass fraction of the High-T cycle solution. Because of the coupling working mode and the inter-restricted relationship between the High-T cycle and Low-T cycle as forgoing description in Section 2.2, the feasible ammonia mass fractions for the Low-T cycle solution should be larger than 0.6, while the ammonia mass fractions of the High-T cycle solution should be in the range between 0.3 and the mass fraction value of the used Low-T cycle solution, leading to relatively lower turbine inlet pressure in double-effect APG cycle, e.g. the maximum achievable pressure when using 100.0 °C boiling temperature is just about 20.0 bar.

Unlike the KCS-11, the power output shown in Fig. 13(a) increases almost linearly with the increasing ammonia mass fraction of the High-T cycle solution when the ammonia mass fraction of the Low-T cycle solution keeps constant, and this increasing rate is larger when the turbine inlet pressure is higher or the ammonia mass fraction of Low-T cycle solution is lower. The energy efficiency and exergy efficiency shown in Fig. 13(b) and (c) increase with the increase of turbine inlet pressure and the decrease of ammonia mass fraction of the Low-T cycle solution, but the efficiencies are insensitive to the change of the ammonia mass fraction of High-T cycle solution. When using 100.0 °C boiling temperature and 20.0 bar turbine inlet pressure, the maximum energy efficiency of the double-effect APG cycle is about 0.142 ($w_{bas,H}$ = 0.6, $w_{bas,L}$ = 0.9) which is about 7.6% higher than that maximum value of KCS-11 under the same operation condition. Almost the same improvement can be achieved in terms of exergy efficiency, i.e. 0.71 with double-effect APG compared to the 0.66 in KCS-11. Another advantage of double-effect APG cycle over its rival is that the maximal efficiencies of double-effect APG cycle are generally accompanied with the maximum power output, namely, there is no trade-off concern when deciding the optimal operational conditions.

As shown in Fig. 13(b), on the basis of best energy efficiency, 20.0 bar turbine inlet pressure and 0.9 mass fraction of the Low-T cycle solution is believed to be the optimal working condition of the double-effect APG cycle at 100.0 °C boiling temperature. Such optimal working conditions have been identified for the boiling temperature range of 100.0–140.0 °C to conduct the comparison between the double-effect APG cycle and KCS-11 as shown in Fig. 14, where each curve represents the varying profile of the energy efficiency against the power output in the optimal case. The superiority of the double-effect APG cycle to KCS-11 is amplified when the boiling temperature is higher, and the improvement is about 3.6–12.6%, 10.7–28.2% and 19–900% respectively when using 100.0 °C, 120.0 °C and 140.0 °C boiling temperature. Moreover, the double-effect APG cycle also benefits from the relatively lower turbine inlet pressure for more reliable operation and easier turbine maintenance. Nevertheless, due to the allowance of using ammonia-richer solution in the boiler, the KCS-11 can generate more power than the double-effect APG cycle does with the same boiling temperature and the same mass flow rate of the basic working solution, as can be seen from Fig. 14.

3.3. Half-effect APG cycle

Fig. 15(a) and (b) show the power output and energy efficiency of the half-effect APG cycle using 100.0 °C boiling temperature and 30.0 bar turbine inlet pressure. Apparently, increasing the mass fraction of the High-P cycle solution, $w_{bas,H,}$ in the H-Boiler results in higher flow rate of the vapour for the turbine, further leading to the increase of power output and energy efficiency. Meanwhile, lowering the ammonia mass fraction of the Low-P cycle solution, $w_{bas,L,}$ leads to the lower backpressure for the turbine, as a result of which larger pressure ratio is created for vapour expansion and therefore more power output can be expected. However, because the vapour quality of the turbine exhaust is required at least 0.9, it becomes meaningless to further reduce the $w_{bas,L}$ in the interest of improving the power output when the low backpressure causes the overexpansion. This explains the dropping energy efficiency at $w_{bas,L}$ = 0.3 shown in Fig. 15(b).

Fig. 15 indicates there is an optimal $w_{bas,L}$ for half-effect APG cycle with a given boiling temperature and turbine inlet pressure, e.g. the optimal $w_{bas,L}$ under the condition exemplified in Fig. 15(b)

Table 2
The energy efficiencies and power outputs when pursuing maximum efficiency and maximum power output of KCS-11.

T_{boi}	P_{tur} = 30 bar				P_{tur} = 20 bar				P_{tur} = 10 bar			
	$\eta_{en,max}$	$\dot{W}_{tur}$	η_{en}	$\dot{W}_{tub,max}$	$\eta_{en,max}$	$\dot{W}_{tur}$	η_{en}	$\dot{W}_{tur,max}$	$\eta_{en,max}$	$\dot{W}_{tur}$	η_{en}	$\dot{W}_{tur,max}$
100 °C	0.132	396.1	0.109	1469.2	0.132	273.2	0.075	1033.3	0.139	202.7	0.081	510.0
90 °C	0.122	423.1	0.107	1362.7	0.118	255.2	0.073	994.3	0.123	151.6	0.070	412.0
80 °C	0.111	475.1	0.105	1252.2	0.104	216.2	0.072	934.2	0.105	156.0	0.059	333.6
70 °C	–	–	–	–	0.091	260.3	0.071	872.3	0.088	98.6	0.046	269.1

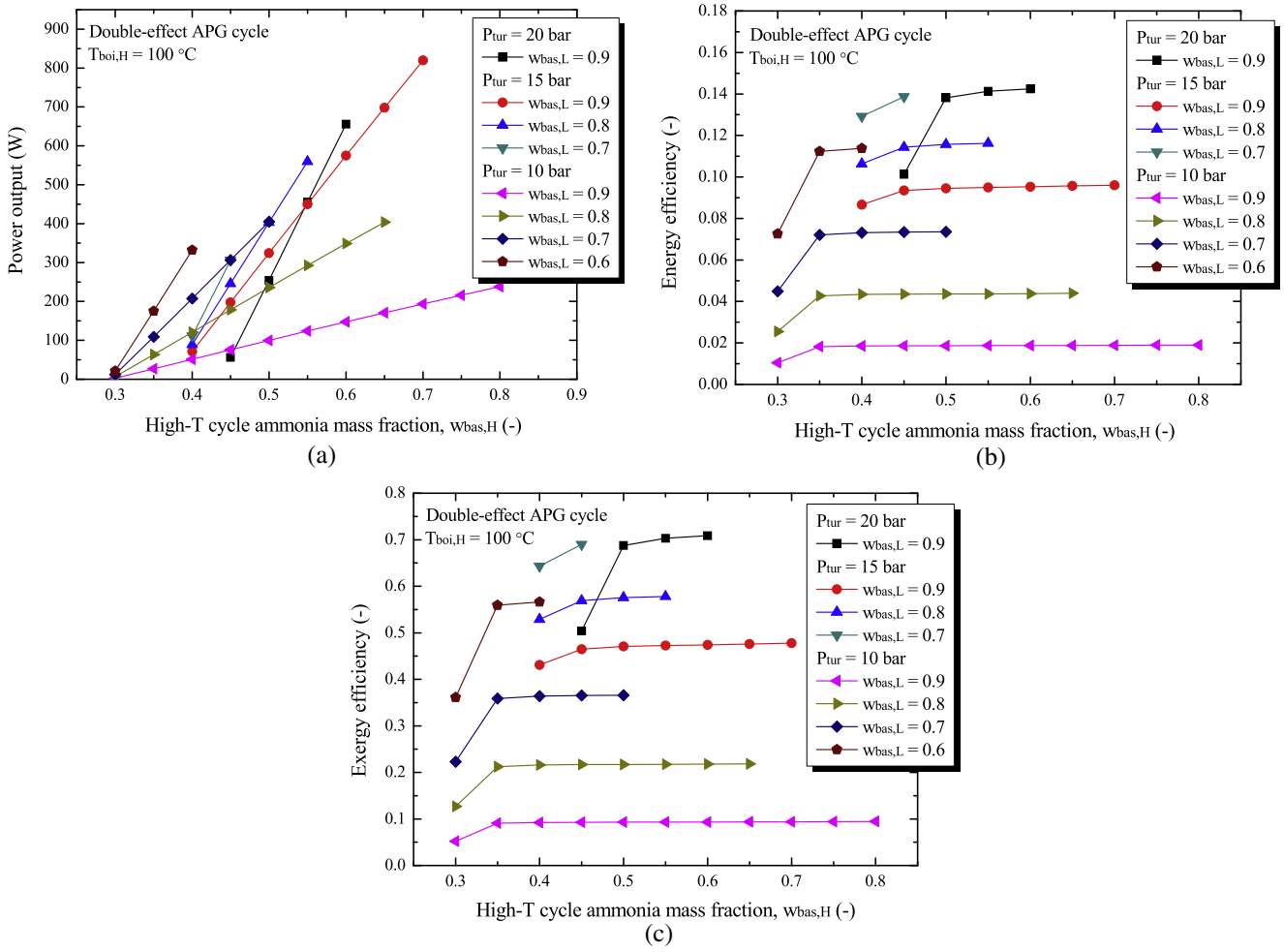

Fig. 13. Performance of double-effect APG cycle at 100.0 °C boiling temperature, (a) power output; (b) energy efficiency; (c) exergy efficiency.

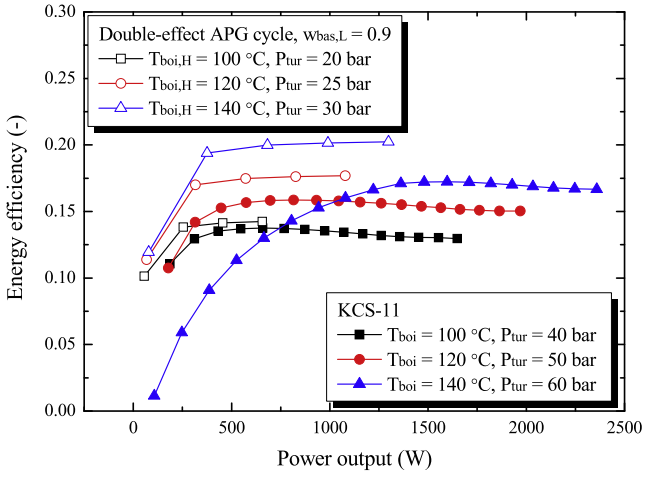

Fig. 14. Energy efficiencies against power output of double-effect APG cycle and KCS-11 at optimal working conditions for different boiling temperatures.

is 0.4. Likewise, other optimal mass fraction values of the Low-P cycle solution have been identified as 0.6, 0.35 and 0.3 for 40.0 bar, 20.0 bar and 10.0 bar turbine inlet pressure when using 100.0 °C boiling temperature. The corresponding power output and energy efficiency of those optimal cases are shown in Fig. 16 (a) and (b), respectively. It is found that the case with lower turbine inlet pressure has the lower value of optimal $w_{bas,L}$, leading to larger pressure ratio at optimal $w_{bas,L}$, e.g. P_L = 0.98 bar for 10.0 bar turbine inlet pressure while P_L = 5.13 bar for 40.0 bar turbine inlet pressure respectively at their optimal $w_{bas,L}$. Thus the lower the used turbine inlet pressure is, the higher the power output can be expected as shown in Fig. 16(a). On the other side, lower $w_{bas,L}$ indicates that higher mass flow rate is required by the Low-P cycle solution in order to achieve the mass balance in the whole half-effect cycle, therefore the required boiling heat for the Low-P cycle is increased, which implies more heat input for the whole cycle. The corresponding varying profiles of energy efficiency are plotted in Fig. 16(b), where turbine inlet pressure at 30.0 bar and optimal $w_{bas,L}$ at 0.4 seems to be the best choice for half-effect APG cycle when using 100.0 °C boiling temperature. In this instance, the maximum energy efficiency can be obtained at 0.086 if the $w_{bas,H}$ is 0.85; alternatively, the maximum power output can be obtained by using $w_{bas,H}$ as high as possible.

Likewise, the best turbine inlet pressure and the optimal $w_{bas,L}$ value were identified when using different boiling temperatures in the half-effect cycle. Fig. 17 shows the optimal energy efficiency of the half-effect cycles using different boiling temperature in comparison with the optimal cases of KCS-11 with the same heat sources. The half-effect cycle is capable of generating 50.0–85.0% more power than KCS-11 is due to the larger pressure ratio; however it requires dual boiling heat input for both High-P and Low-P cycles, consequently, its energy efficiencies are about 35.0–45.0%, 25.0–35.0% and 4.0–30.0% lower than those of KCS-11 using 100.0 °C, 80.0 °C and 60.0 °C boiling temperature respectively.

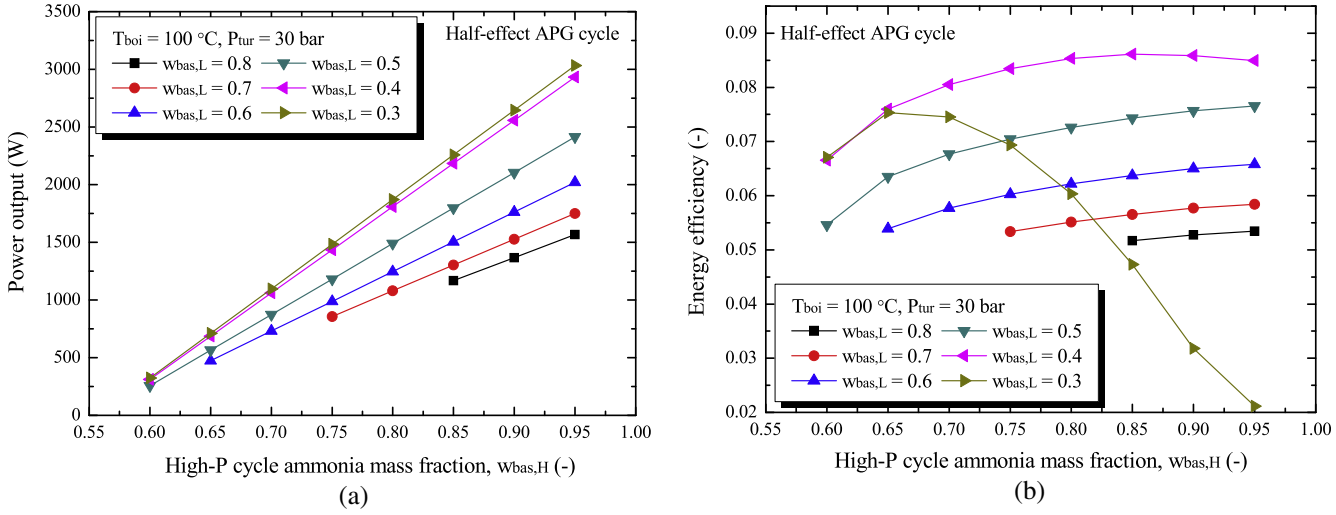

Fig. 15. Performance of half-effect APG cycle at 100.0 °C boiling temperature and 30.0 bar turbine inlet pressure, (a) power output; (b) energy efficiency.

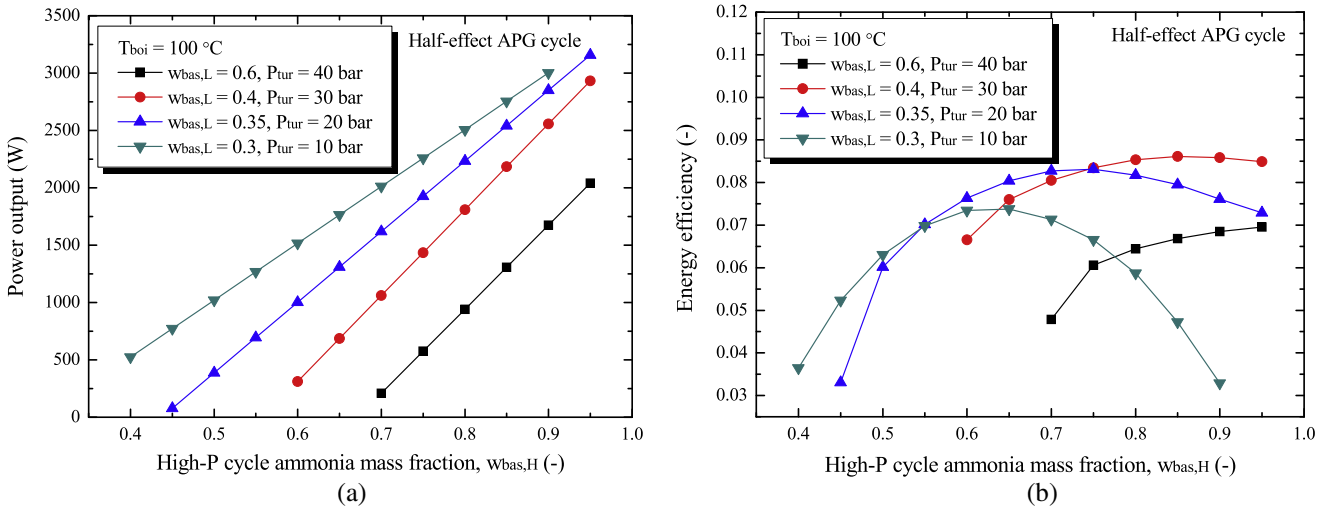

Fig. 16. Optimal performance of half-effect APG cycle at 100.0 °C boiling temperature and different turbine inlet pressures, (a) power output; (b) energy efficiency.

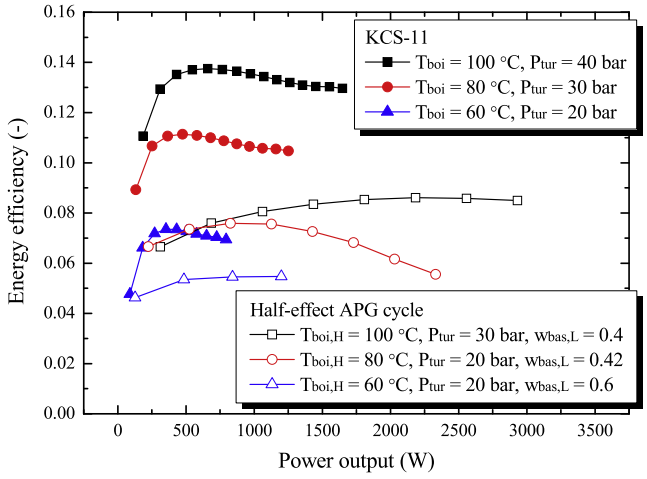

Fig. 17. Energy efficiencies against power output of half-effect APG cycle and KCS-11 at optimal working conditions for different boiling temperatures.

3.4. Ejector-combined APG cycle

By using an ejector, the backpressure of the turbine can be reduced while the condensation pressure remains the same. The energy efficiency of ejector-combined APG cycle is improved compared to KCS-11, as being exemplified in Fig. 18 when using 100.0 °C boiling temperature. To ensure the effective ejector operation, the ammonia mass fraction of the basic solution should not be too high, otherwise the flow rate of the high-pressure primary flow in the ejector is not sufficient to entrain the low-pressure secondary flow to a medium-pressure level. Hence, the allowed highest ammonia mass fractions in ejector-combined APG cycle are lower than those of KCS-11. It is noteworthy that if the basic solution has higher ammonia mass fraction, the high-pressure primary flow is at lower flow rate; in this case, the turbine backpressure created by the ejector is not distinctively lower than the condensation pressure, consequently the efficiency is hardly improved, e.g. the cases with 100.0 °C boiling temperature, larger than 0.7 ammonia mass fraction and 30.0 bar turbine inlet pressure in Fig. 18 have almost the same energy efficiency with those of KCS-11. It is evident in Fig. 18 that there exists the optimal value of ammonia mass fraction where the cycle using the ejector accomplishes the most

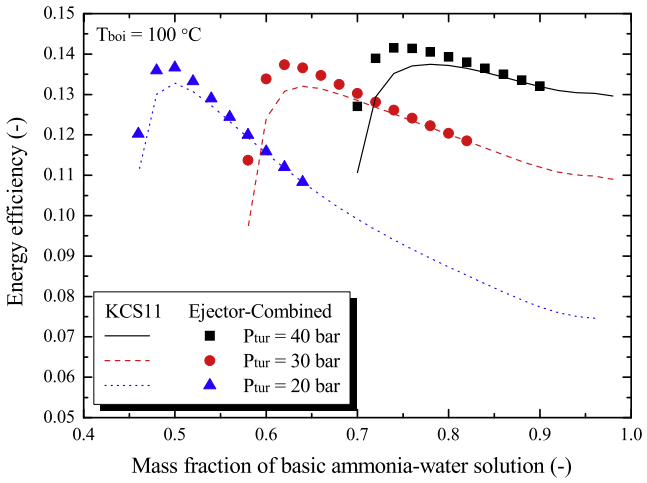

Fig. 18. Energy efficiencies against ammonia mass fraction of ejector-combined APG cycle and KCS-11 at 100.0 °C boiling temperature.

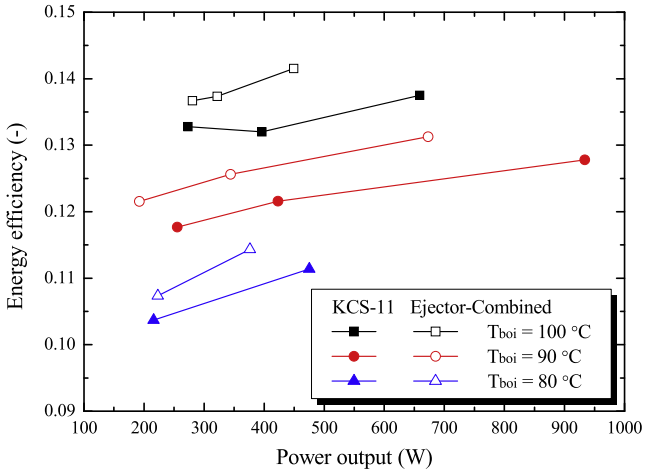

Fig. 19. Optimal energy efficiencies against power output of ejector-combined APG cycle and KCS-11 at different boiling temperature and turbine inlet pressure.

distinctive improvement as it has the maximum energy efficiency, which is 3.5–5.0% higher than KCS-11 using the same basic working solution.

Fig. 19 compares the energy efficiency and power output of ejector-combined APG cycle to those of KCS-11 while both use the optimal ammonia mass fractions under different boiling temperature and turbine inlet pressure. Based on the same power output, combining the ejector can improve the energy efficiency by 2.9–6.8%, 4.3–5.2% and 3.2–5.2% for 100.0 °C, 90.0 °C and 80.0 °C boiling temperature, respectively; whereas, if based on the maximum energy efficiency, the optimal value of ammonia mass faction in ejector-combined cycle is lower than that of KCS-11, meaning less ammonia vapour can be generated for power generation, hence the former one has lower power output capacity. Of course, as the foregoing discussion on KCS-11 in Section 3.1, one can pursue the maximum power output by slightly compromising the energy and exergy efficiencies.

4. Conclusions

The present paper explored advanced absorption power generation (APG) cycles, one double-effect APG cycle, one half-effect APG cycle and one ejector-combined APG cycle have been evaluated using KCS-11 as the basic cycle. The performance of these advanced APG cycles, including power output, energy and exergy efficiencies, have been numerically analyzed and compared with KCS-11 as a benchmark. Each advanced APG cycle had its advantages at some aspects but shortcomings at other aspects. The exploration of these advanced APG cycles enriched the category of ammonia power generation cycles and their superiorities may inspire further numerical and experimental studies. The primary findings of this paper are made as follows.

(a) The double-effect APG cycle can largely improve the energy and exergy efficiencies especially when the boiling temperature was high, the improvement is about 3.6–12.6%, 10.7–28.2% and 19–900% respectively when using 100.0 °C, 120.0 °C and 140.0 °C boiling temperature; however, its power output capacity was lower.
(b) The half-effect APG cycle exhibited better performance in terms of power output capacity as it is capable of generating 50.0–85.0% more power than KCS-11; however its energy and exergy efficiencies were compromised.
(c) The ejector-combined APG cycle replacing the throttling valve and mixer in the KCS-11 by an ejector can have more than 5% improvement on the energy and exergy efficiencies without using a bulky two sets KCS-11; however, the power output capacity was lower at the optimal operation condition.

Acknowledgement

The authors gratefully acknowledge the support from the IDRIST project (EP/M008088/1) and Heat-STRESS project (EP/N02155X/1), funded by the Engineering and Physical Science Research Council of UK. Data supporting this publication is openly available under an 'Open Data Commons Open Database License'. Additional metadata are available at: http://dx.doi.org/10.17634/148532-5. Please contact Newcastle Research Data Service at rdm@ncl.ac.uk for access instructions.

References

[1] Ammar Y, Joyce S, Norman R, Wang YD, Roskilly AP. Low grade thermal energy sources and uses from the process industry in the UK. Appl Energy 2012;89:3–20.
[2] Chen H, Goswami DY, Stefanakos EK. A review of thermodynamic cycles and working fluids for the conversion of low-grade heat. Renew Sustain Energy Rev 2010;14:3059–67.
[3] Zhang X, He M, Zhang Y. A review of research on Kalina cycle. Renew Sustain Energy Rev 2012;16:5309–18.
[4] Ayou DS, Bruno JC, Saravanan R, Coronas A. An overview of combined absorption power and cooling cycles. Renew Sustain Energy Rev 2013;21:728–48.
[5] Maloney JD, Robertson RC. Thermodynamic study of ammonia-water heat power cycles. Oak Ridge National Laboratory Report CF-53-8-43; 1953.
[6] Kalina AI. Combined cycle and waste heat recovery power systems based on a novel thermodynamic energy cycle utilizing low-temperature heat for power generation. American Society of Mechanical Engineers, Paper 83-JPGC-GT-3; 1983.
[7] Kalina AI, Leibowitz HM. Applying Kalina technology to a bottoming cycle for utility combined cycles. American Society of Mechanical Engineers, Paper 87-GT-35; 1987.
[8] Ibrahim OM, Klein SA. Absorption power cycles. Energy 1996;21:21–7.
[9] Hettiarachchi HDM, Golubovic M, Worek WM, Ikegami Y. The performance of the Kalina cycle system 11 (KCS-11) with low-temperature heat sources. J Energy Res Technol 2007;129:243–7.
[10] Sun F, Ikegami Y, Jia B. A study on Kalina solar system with an auxiliary superheater. Renewable Energy 2012;41:210–9.
[11] Sun F, Ikegami Y, Arima H, Zhou W. Performance analysis of the low-temperature solar-boosted power generation system 12 – Part I: comparison between Kalina solar system and Rankine system. J Sol Energy Eng 2013;135:011006.

[12] Sun F, Zhou W, Ikegami Y, Nakagami K, Su X. Energy-exergy analysis and optimization of the solar-boosted Kalina cycle system (KCS-11). Renewable Energy 2014;66:268–79.
[13] Singh OK, Kaushik SC. Energy and exergy analysis and optimization of Kalina cycle coupled with a coal fired steam power plant. Appl Therm Eng 2013;51:787–800.
[14] Elsayed A, Embaye M, AL-Dadah R, Mahmoud S, Rezk A. Thermodynamic performance of Kalina cycle system 11 (KCS11): feasibility of using alternative zeotropic mixtures. Int J Low-Carbon Technol 2013;8:i69–78.
[15] He J, Liu C, Xu X, Li Y, Wu S, Xu J. Performance research on modified KCS (Kalina cycle system) 11 without throttle valve. Energy 2014;64:389–97.
[16] Mlcak H, Mirolli M, Hjartarson H, Ralph M. Notes from the north: a report on the debut year of the 2 MW Kalina cycle® geothermal power plants in Húsavík, Iceland. Trans – Geoth Resour Counc 2002;26:715–8.
[17] Fu W, Zhu J, Li T, Zhang W, Li J. Comparison of a Kalina cycle based cascade utilization system with an existing organic Rankine cycle based geothermal power system in an oilfield. Appl Therm Eng 2013;58:224–33.
[18] DiPippo R. Second law assessment of binary plants generating power from low-temperature geothermal fluids. Geothermics 2004;33:565–86.
[19] Guzovic Z, Majcen B, Cvetkovic S. Possibilities of electricity generation in the Republic of Croatia from medium-temperature geothermal sources. Appl Energy 2012;98:404–14.
[20] Kang YT, Kunugi Y, Kashiwagi T. Review of advanced absorption cycles: performance improvement and temperature lift enhancement. Int J Refrig 2000;23:388–401.
[21] Srikhirin P, Aphornratana S, Chungpaibulpatana S. A review of absorption refrigeration technologies. Renew Sustain Energy Rev 2001;5:343–72.
[22] Li X, Zhang Q, Li X. A Kalina cycle with ejector. Energy 2013;54:212–9.
[23] El-sayed YM, Tribus M. Thermodynamic properties of water-ammonia mixtures theoretical implementation for use in power cycles analysis. American Society of Mechanical Engineers, Advanced Energy Systems Division (Publication) AES 1985; 1:89–95.
[24] Ziegler B, Trepp Ch. Equation of state for ammonia-water mixtures. Int J Refrig 1984;7:101–6.
[25] Sumeru K, Nasution H, Ani FN. A review on two-phase ejector as an expansion device in vapor compression refrigeration cycle. Renew Sustain Energy Rev 2012;16:4927–37.
[26] Kornhauser AA. The use of an ejector as a refrigeration expander. International Refrigeration and Air Conditioning Conference, Purdue University, USA; 1990.
[27] Cardemil JM, Colle S. A general model for evaluation of vapor ejectors performance for application in refrigeration. Energy Convers Manage 2012;64:79–86.
[28] Kim KH, Kim SW. Assessment of an absorption power cycle for efficient conversion of low-grade heat source. Int J Min, Metall Mech Eng 2014;2:116–20.